IEEE Access
Multidisciplinary | Rapid Review | Open Access Journal

Received October 11, 2019, accepted October 23, 2019, date of publication November 4, 2019, date of current version November 18, 2019.

Digital Object Identifier 10.1109/ACCESS.2019.2951489

Design and Characterization of a Miniaturized Implantable Antenna in a Seven-Layer Brain Phantom

SAMNANG HOUT[1,3] AND JAE-YOUNG CHUNG[2,3], (Senior Member, IEEE)

[1]Department of Integrated IT Engineering, Seoul National University of Science and Technology, Seoul 01811, South Korea
[2]Department of Electrical and Information Engineering, Seoul National University of Science and Technology, Seoul 01811, South Korea
[3]Research Center for Electrical and Information Technology, Seoul National University of Science and Technology, Seoul 01811, South Korea

Corresponding author: Jae-Young Chung (jychung@seoultech.ac.kr)

This work was supported by the Advanced Research Project funded by Seoul National University of Science and Technology (SeoulTech).

ABSTRACT In this paper, we propose a miniaturized implantable antenna exhibiting a broadside radiation pattern and wide operating bandwidth. Previously reported small implantable antennas often display omni-directional radiation patterns which are not suitable for in-to-off wireless body area network. The proposed design overcomes this problem by optimizing the antenna structure inside a realistic brain implant environment, a seven-layer brain phantom including skin, fat, bone, dura, cerebrospinal fluid (CSF), gray and white matters. The seven-layer phantom was modeled in a full-wave simulation software, and then the antenna was embedded in dura layer. The antenna has a circular shape with a diameter of 10 mm and a thickness of 0.5 mm. The top and bottom insulating layers share the same dimensions of the antenna. With the given location and surrounding materials, the antenna geometry was optimized to resonate at 2.4 GHz and to radiate broadside. The optimal design was fabricated using a low-loss biocompatible PCB material, Taconic RF-35 ($\varepsilon_r = 3.5$, $\tan\delta = 0.0018$), and tested in a seven-layer brain phantom implemented with semi-solid artificial tissue emulating (ATE) materials. The results of both the simulation and measurement revealed similar -10-dB impedance bandwidths of 13.8% and 14.9%, respectively, which are wider than those of most single-band implantable antennas operating at 2.4 GHz. The proposed antenna also displayed a measured peak realized gain of -20.75 dBi and an acceptable radiation efficiency of 0.24%, which are within the typical range. Furthermore, we calculated the specific absorption rate (SAR) and assessed its compliance with the IEEE safety guidelines.

INDEX TERMS Artificial tissue emulating (ATE) materials, broadside radiation pattern, implantable antenna, in-vitro testing, seven-layer brain phantom, specific absorption rate (SAR).

I. INTRODUCTION

Brain implant devices are designed to help both patients living with brain diseases and people with perspective neurological disorders during therapy and early diagnosis, respectively. For example, some applications of the brain implant technology include restoring lost sensory information from a disease [1] and early detection of epileptic seizures [2]. However, brain implant devices typically use wires to connect with external units that can threaten safety of the patients and limit their movements [2], [3]. Therefore, more attention has now turned toward wireless devices. Many works on wireless brain implant devices are reported in [2]–[7]. In a wireless brain implant system, a miniaturized and efficient antenna is needed for effective communication with an external device.

Fig. 1 shows the concept of a wireless brain monitoring device. A neural recorder is connected to an implantable antenna for transmitting brain signals to an external receiver located above the head. The implantable antenna should have a broadside radiation pattern so that it can provide a strong signal that can be easily detected by the receiver outside [8], [9]. However, the main problem with an implantable antenna is that it is an electrically small antenna typically displaying an omni-directional radiation pattern. Brain-implanted antennas, such as those reported in [10]–[13], radiate either omni-directional or asymmetrical radiation

The associate editor coordinating the review of this manuscript and approving it for publication was Shah Nawaz Burokur.

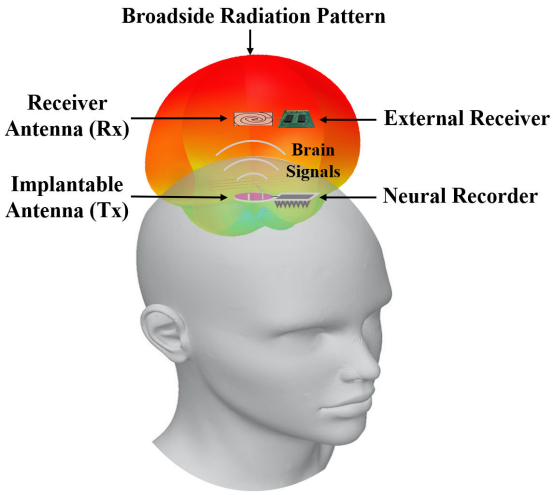

FIGURE 1. An overview of the implantable antenna's role in transmitting brain signals in the wireless brain monitoring device.

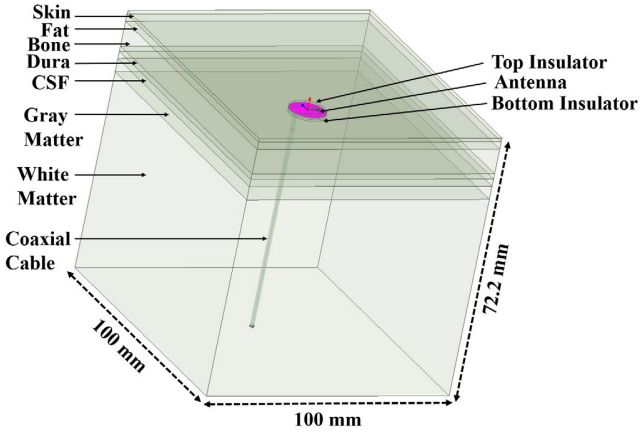

FIGURE 2. Simulation setup showing the implantable antenna implanted inside the seven-layer brain model mimicking the human brain.

TABLE 1. Electrical properties of brain tissues at 2.4 GHz and their thickness.

Tissue	Relative Permittivity	Loss Tangent	Thickness (mm)
Skin	42.923	0.273	1
Fat	5.285	0.145	2
Cortical Bone	11.410	0.252	7
Dura	42.099	0.292	1.5
CSF	66.319	0.385	2
Gray Matter	48.994	0.271	3.7
White Matter	36.226	0.246	55

patterns, which are not favored in this brain signal transmitting application as the RF signals at the back lobe are not used for this communication and may also increase specific absorption rate (SAR) in surrounding brain tissues.

Kiourti and Nikita [9] shows that the radiation pattern of an implantable antenna is related to the surrounding biological tissues. They have unique dielectric properties resulting in different RF interactions with electromagnetic waves generated by the implanted antenna [14]. Therefore, it is crucial to design the antenna within the correct brain model.

In this paper, the antenna was implanted in a seven-layer brain phantom, and then its structure was optimized to resonate at the industrial-scientific-medical (ISM) 2.4 GHz band and to radiate broadside as in Fig. 1. The transverse area of the seven-layer phantom was 100 mm × 100 mm, sufficiently large to avoid edge diffractions, and the total thickness was 72.2 mm where each layer's thickness and material properties were determined by [15] and [16], respectively as in Section II. The phantom was fabricated with semi-solid artificial tissue emulating (ATE) materials followed by a recipe in [5].

The optimized antenna was also fabricated and then inserted in the phantom for more realistic and reliable in-vitro testing. The measured results were compared with full-wave simulation results in Section III. The reflection coefficient (S_{11}) and antenna radiation pattern were the key parameters for the measurements. From S_{11}, the antenna's operation frequency and bandwidth could be determined. With the radiation pattern, the antenna's directivity, peak gain and radiation efficiency could be found. In particular, the radiation pattern is the most crucial parameter for the brain implant application since the maximum beam direction should aim to the boresight (i.e., broadside radiation). On top of this, the specific absorption rate (SAR) was calculated to ensure the patient safety. By analyzing SAR in accordance with IEEE standards, the maximum input power limits could be identified. The simulated SAR and input power results were also discussed in Section III.

II. FULL-WAVE ELECTROMAGNETIC SIMULATION

A. THE SEVEN-LAYER BRAIN MODEL

We modeled the seven-layer brain model in a finite-element method (FEM) based full-wave electromagnetic simulation tool, Ansys HFSS. Fig. 2 shows the model made up of seven different lossy brain tissues. Commonly, a six-layer rectangular phantom is often used to model a typical adult brain [4], [8], [14], [17]. However, according to [18], which is the most referred paper for human tissues' electrical properties, the last brain tissue at the bottom contains two different materials, gray and white matters, with different relative permittivity (ε_r) and loss tangent ($\tan\delta$) values. Therefore, we remodeled a more realistic form of the human brain with seven tissue layers. In order of layer, the seven brain tissues were skin, fat, cortical bone (skull), dura, cerebrospinal fluid (CSF), gray matter, and white matter. Table 1 shows the electrical properties (permittivity and loss tangent) at 2.4 GHz and thickness of the brain tissues assigned to the rectangular box in Ansys HFSS for simulation. The values of the permittivity and loss tangent were those of real brain tissues sourced

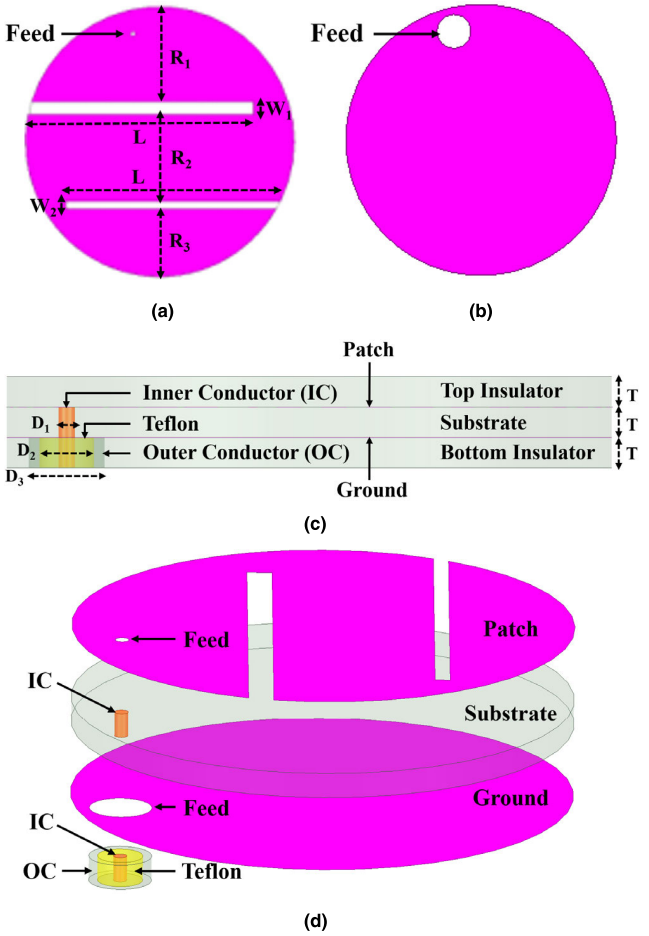

FIGURE 3. Geometry of the proposed implantable antenna : (a) top circular patch, (b) bottom ground plane, (c) side view, and (d) exploded view without top and bottom insulators.

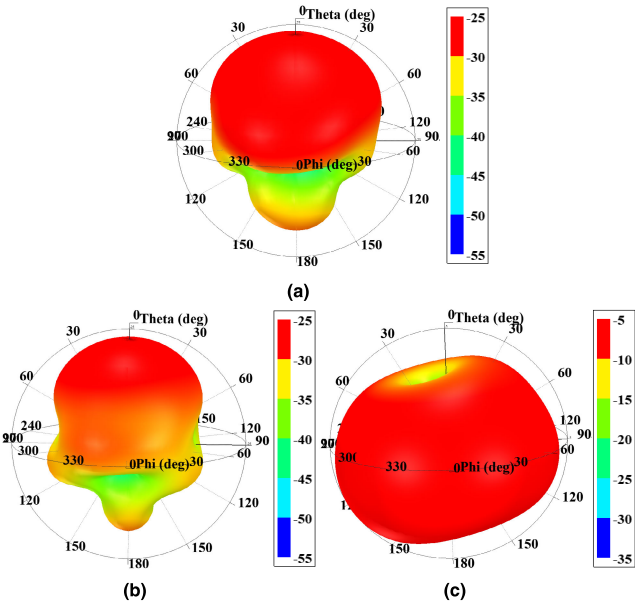

FIGURE 4. Simulated radiation patterns of the proposed antenna inside (a) the seven-layer brain model, (b) the six-layer brain model, and (c) free space.

from [16], and the thickness of each brain tissue was chosen from that of a typical adult brain in [15]. As can be seen, the bottom layers of this seven-layer brain model, such as the gray and white matters, had high permittivity and thickness that can reflect and absorb some of the antenna radiated waves [14].

Depicted in Fig. 2 is the simulation setup carried out by using finite-element method (FEM) in Ansys HFSS. An implantable antenna together with top and bottom insulating layers is located in between bone and dura. Such implant location was chosen for better radiation efficiency [1]. The antenna placed in dura, where the bone exhibits low conductivity, can facilitate RF power transmission with lower losses, hence enhancing radiation efficiency.

B. ANTENNA DESIGN AND OPTIMIZATION

Fig. 3(a) and (b) show top and bottom sides of the proposed implantable antenna. It has a form of circular patch antenna excited from the bottom. The substrate used is Taconic RF-35 ($\varepsilon_r = 3.5$, $\tan\delta = 0.0018$). Several previous works such as [11]–[13] have popularly utilized high permittivity Rogers 3210 ($\varepsilon_r = 10.2$, $\tan\delta = 0.003$) for miniaturization. However, a higher permittivity often accompanies a higher quality factor, resulting in narrower bandwidth and lower radiation efficiency. For the present work, we selected the low permittivity and low-loss biocompatible substrate. For miniaturization, an offset-fed meander antenna with two slots was printed for elongating the antenna's electrical length, effectively decreasing the resonant frequency [9]. The diameter and thickness (T) of the antenna are 10 mm and 0.5 mm, respectively.

With regard to biocompatibility, it is essential that the implantable antenna is covered with insulating layers to avoid direct contact with brain tissues, both for patient safety and implant robustness. To achieve this, low-loss materials such as silicon ($\varepsilon_r = 3.1$, $\tan\delta = 0.0025$) are widely used [19]. For simplicity, we used the same biocompatible substrate material, Taconic RF-35, for both top and bottom insulators. The insulating layers have 0.5-mm thickness, the original substrate thickness, for ease of prototype fabrication. Aside from using biocompatible materials, antenna shape also plays an important role in securing patient safety, especially in protecting the surrounding implant tissues. Instead of a rectangular or square geometry, we selected a circular shape for our antenna design as such has no sharp edges that can damage the nearby biological tissues [20].

Fig. 3(c) shows a side view of the antenna sandwiched by the top and bottom insulators. The conductive circular patch and ground were printed on the top and bottom surfaces of substrate, respectively, as depicted in Fig. 3(d). To feed the antenna, inner/outer conductors and Teflon of a standard RF coaxial cable were designed in the simulation model which is the same configuration to the antenna prototype used in the in-vitro testing discussed in Section III.

TABLE 2. Parameters of the antenna.

Parameter	Value (unit: mm)
R_1	3.5
R_2	3.2
R_3	2.5
W_1	0.5
W_2	0.3
L	8.5
D_1	0.27
D_2	0.9
D_3	1.25
T	0.5

As the antenna's far-field radiation pattern changes relative to implant environments [9], the antenna model must be optimized according to its surrounding brain model. The brain model must resemble a real human brain as much as possible to keep the optimized broadside directivity of the antenna unchanged even while implanted inside an eventual human brain. Fig. 4(a) shows the 3D antenna radiation pattern when the proposed antenna geometry is optimized in the seven-layer brain model. It is obviously broadside radiating with a low back-lobe. However, the back-lobe and side-lobe level increase when the same antenna is implanted in the six-layer model as shown in Fig. 4(b). If the antenna is in free-space, the radiation pattern becomes omni-directional as in Fig. 4(c), showing the strong dependence of antenna radiation on the surrounding environments.

C. PARAMETRIC ANALYSIS

We conducted a parametric analysis by simulating the antenna model inside a human brain environment (described in Section A) and by varying the values of key parameters such as slot length (L) and widths (W_1, W_2) to understand their effects on the reflection coefficient (S_{11}). This study can further optimize the antenna design to work at our desired operating frequency of 2.4 GHz. Other parameters such as R_1, R_2, and R_3were just dependent variables of the key parameters L, W_1, W_2; therefore, they were not included in this study.

The proposed antenna configuration consists of top and bottom insulators, and a substrate with a circular patch and a ground plane. Each has a 10-mm diameter and 0.5-mm thickness (T). The details of the design are provided in Fig. 3(a) to (d), and the proposed values of all parameters are presented in Table 2.

We conducted a parametric analysis of the slot length (L) first. On the basis of the results, the resonance frequency of the antenna changed significantly with L, as can be seen in Fig. 5(a), dropping to lower bands as L increased. We selected L = 8.5 mm, which complements the approximately 2.4-GHz operating frequency of the antenna. Subsequently, we varied slot widths (W_1, W_2), whose effects

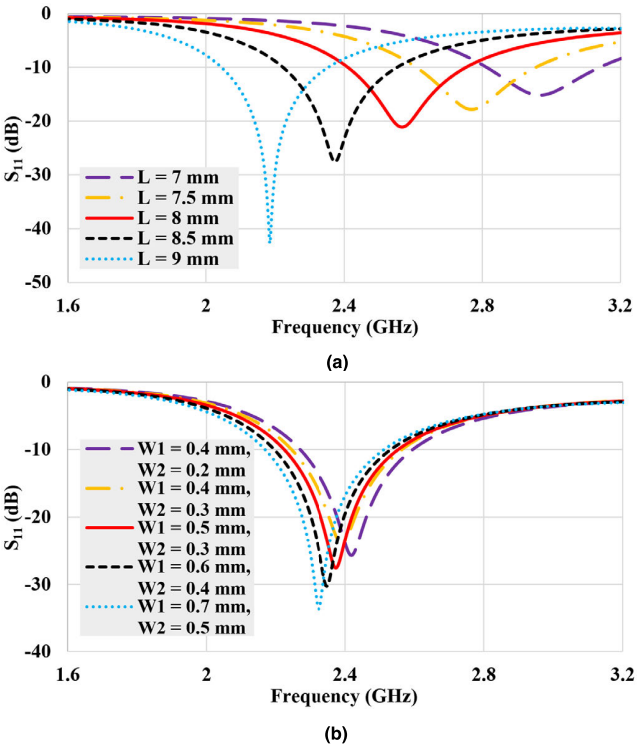

FIGURE 5. Comparisons of reflection coefficient (S_{11}) for (a) different slot lengths (L), and (b) different slot widths (W_1, W_2).

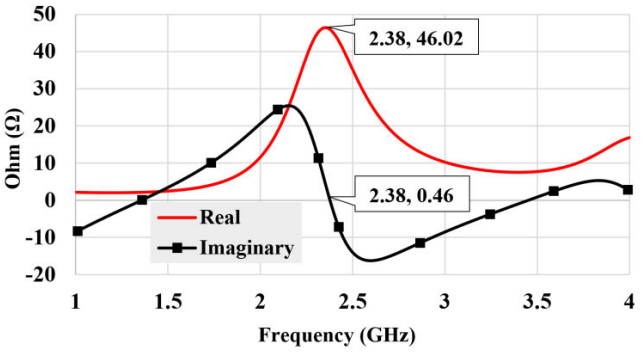

FIGURE 6. Input impedance (Z_{in}) of the proposed antenna design.

on the reflection coefficient (S_{11}) seemed minor, as indicated in Fig. 5(b). After taking into account the important criteria for optimal antenna performance at the proposed 2.4-GHz operating frequency such as a satisfactory −10-dB reflection coefficient (S_{11}) and resonance frequency, we chose W_1 = 0.5 mm and W_2 = 0.3 mm. Such antenna design with the proposed parametric values had almost perfect impedance matching of 50 Ω and the closest resonance frequency to 2.4 GHz. As shown in Fig. 6, the proposed antenna had an input impedance (Z_{in}) of 46.02 + j 0.46 Ω at the resonance frequency of 2.38 GHz. However, the parameters include, but were not limited to, these proposed values based on different scenarios, which implies that the antenna design can be easily tuned in other implant locations and applications under similar frequency bands.

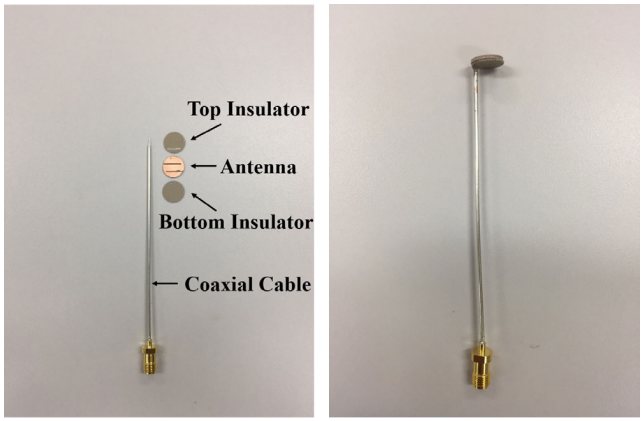

FIGURE 7. The proposed antenna prototype (a) before assembly, and (b) after assembly, by means of soldering and gluing.

III. ANTENNA FABRICATION AND MEASUREMENT

A. PROTOTYPE FABRICATION

We carefully fabricated our proposed implantable antenna prototypes in the laboratory by means of photolithography. The photolithographic process was performed to remove metallization from the slots on the circular patch. The entire copper of Taconic RF-35 substrate (thickness T = 0.5 mm) was etched off using the same process to achieve the insulating layers. Afterward, an antenna prototype was connected to an SMA coaxial cable by means of a soldering process and then finally glued with top and bottom insulators for bonding purposes. The final configuration of a fabricated antenna prototype is shown in Fig. 7.

B. BRAIN PHANTOM FABRICATION

Certain steps such as formulating a brain phantom and measuring its electrical properties should be carried out prior to an in-vitro testing of an implantable antenna. A brain phantom consists of semi-solid ATE materials placed on top of each other to create seven layers (skin, fat, bone, dura, CSF, gray matter, and white matter) similarly as in the simulation brain environment. We fabricated the ATE materials for each layer using chemical substances such as deionized water, sodium chloride (NaCl), agar, boric acid, TX-151, and polyethylene (LDPE) powder. The concentration of each chemical ingredient for the fabrication is given in Table 3.

The ingredients in Table 3 were for characteristics of ATE materials mimicking the electrical properties of real biological tissues at 2.4 GHz. Most of these values were taken from [5]. However, in terms of the amount of deionized water and LDPE powder, we modified the original formulas for skin and white matter to obtain a better match of the electrical properties of real skin and white matter tissues at 2.4 GHz. Accordingly for fat, dura, and CSF, we decided on the amount of chemical ingredients via a trial-and-error method until ATE materials with the same electrical properties as real fat, dura, and CSF tissues were produced.

TABLE 3. Ingredient concentrations of ATE materials at 2.4 GHz(Unit: %).

Ingredient	Deionized Water	NaCl	Agar	Boric Acid	TX-151	LDPE Powder
Skin	75.4	0.1	3.9	1.2	3.2	16.2
Fat	39.3	0.001	4.9	1.5	4.9	49.4
Bone	49.3	0.001	4.9	1.5	4.9	39.4
Dura	75.2	0.1	4.5	1.4	3.8	15
CSF	80.2	0.1	4.5	1.4	3.8	10
Gray Matter	75.2	0.1	4.5	1.4	3.8	15
White Matter	69.6	0.1	5.6	1.0	3.9	19.8

FIGURE 8. The fabricated seven-layer brain phantom.

For ATE material fabrication, we adopted the process stated in [21]. Thus, we prepared fabrication equipment, including a spatula, a stainless-steel pot, a portable electric stove, a digital scale, masks, and gloves, and then proceeded with the laboratory hands-on fabrication. To validate our results, we measured the permittivity and loss tangent of the fabricated ATE materials using an open-ended coaxial probe (OECP) and then compared the measured values with those in reference [16]. Both results showed a reasonably good agreement. Finally, we constructed the seven-layer brain phantom (Fig. 8) by assembling the fabricated semi-solid ATE materials based on their thickness and layer order.

C. IN-VITRO MEASUREMENT RESULTS

Furthermore, we verified the measurement results with numerical simulations by conducting an in-vitro testing to check the performance of the fabricated antenna prototype inside the constructed seven-layer ATE brain phantom, which emulates biological brain tissues. The antenna prototype was first immersed at a location inside the brain phantom based on the same scenario as that with the simulation environment in Ansoft HFSS (Fig. 2). The prototype was then connected to an Anritsu MS2038C vector network analyzer (VNA) for measurement of the reflection coefficient (S_{11}) from 1 to 4 GHz. Fig. 9(a) demonstrates the experimental setup.

Subsequently, we compared the simulated and measured reflection coefficients (S_{11}), as displayed in Fig. 10(a). Note that the antenna resonated at 2.38 GHz in the simulation and 2.47 GHz in the measurement where the error between the simulated and measured results was 3.8%. Such frequency

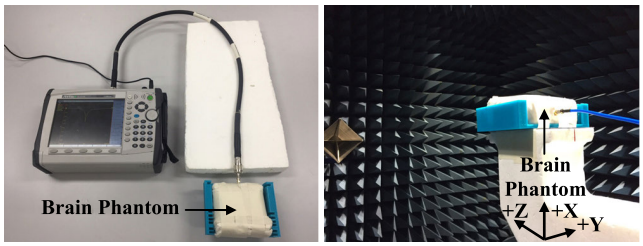

FIGURE 9. Measurement setup of the implantable antenna prototype inside the constructed seven-layer brain phantom: (a) reflection coefficient (S_{11}) measurement, and (b) radiation pattern measurement in the anechoic chamber.

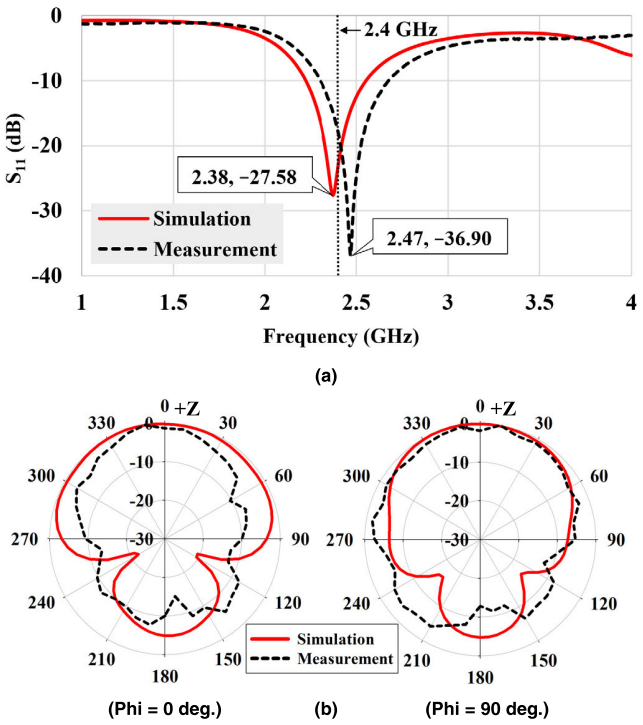

FIGURE 10. (a) Comparison between the simulation and measurement for S_{11}. (b) Normalized radiation patterns (in dB) of the simulation and measurement at 2.4 GHz.

shift was caused by an air gap between the antenna and the top/bottom insulators attached to each other by glue. According to [22], there is always an air gap in the glue layer, which can be avoided only with the use of a highly accurate fabricating machine. Furthermore, such deviation could be attributed to the residual error in HFSS numerical solutions and parasitic effects from soldering the SMA coaxial cable to the antenna [8]. Despite this issue, both the simulated and measured results demonstrated a good agreement, where the −10-dB bandwidth of the reflection coefficient (S_{11}) in both cases covered our frequency of interest (2.4 GHz). The simulated and measured bandwidths of the proposed antenna ranged from 2.22 to 2.55 GHz and from 2.30 to 2.67GHz, respectively. An implantable antenna with a wide bandwidth is very much needed to ensure a stable impedance matching and withstand the frequency shift due

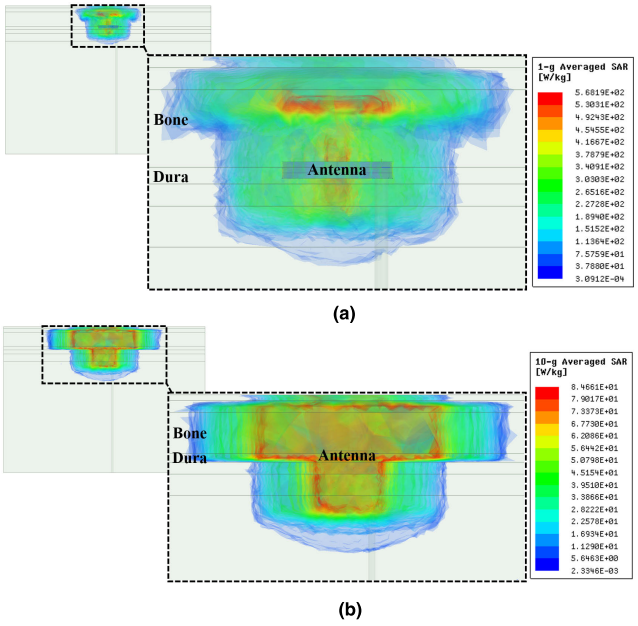

FIGURE 11. Simulated $SAR_{average}$ values for all layers of the seven-layer brain model at 2.4 GHz: (a) SAR_{1g}, and (b) SAR_{10g}.

to the change in implanted environment from one person to another [23], [24]. Bandwidths of the proposed antenna were 330 MHz (13.8%) in the simulation case and 370 MHz (14.9%) in the measurement case, both of which are larger than those of many single-band implantable antennas operating at 2.4 GHz (e.g., [25]–[27]) reported in the literature (refer to Table 5).

We tested the radiation performance of the antenna inside the seven-layer brain phantom inside an anechoic chamber, as depicted in Fig. 9(b). During the measurement, the antenna was placed on a rotational positioner which rotated 360° around +Z axis and moved 180° horizontally from −Y to +Y axis to compute Phi (ϕ) and Theta (θ) components of the radiated signals, respectively. Consequently, the proposed antenna achieved a measured peak realized gain of −20.75 dBi with a radiation efficiency of 0.24%. A low gain is common for implantable antennas, as shown in Table 5, because of their small sizes and the surrounding lossy implant tissues, and low-radiation efficiency is acceptable when applying low-power transmission such as this application. Fig. 10(b) shows plots of the normalized radiation patterns in decibels (dB) at 2.4 GHz, in which apparently the maximum radiation moved along the +Z axis toward the top of the head where an external receiver was supposedly located. A similarity between the simulated and measured radiation patterns was also easily observed.

By principle, the radiation characteristics of an implantable antenna affect patient safety. When an antenna is implanted inside a human brain for neural signal transmission, the surrounding brain tissues absorb the radiating electromagnetic energy, which is potentially harmful to the patient if it exceeds certain levels. Therefore, it is essential to monitor the specific absorption rate (SAR) to preserve patient safety. Technically,

TABLE 4. Simulated maximum average SAR values and maximum allowable net input power at 2.4 GHz.

IEEE Standard	Max Average SAR (W/kg)	Max Net Input Power (mW)
C95.1-1999 (1-g avg)	568.2	2.8
C95.1-2005 (10-g avg)	84.6	23.6

TABLE 5. Performance comparison between the proposed antenna and other implantable antennas operating at 2.4 GHz.

Antenna	Size (mm^3)	Bandwidth (%)	Peak Gain (dBi)	SAR (W/kg)	
				1 g	10 g
Present work	39.3	14.9	−20.75	568.2	84.6
[25]	99.7	12.4	−22.7	508	-
[26]	127	10.2	−20.4	213	26.6
[27]	127	5.69	−27.2	-	-

SAR values must comply with IEEE C95.1-1999 (United States standard) and IEEE C95.1-2005 (European Union standard), restricting the maximum average SAR over 1 g of tissue to 1.6 W/kg and over 10 g of tissue to 2 W/kg, respectively [28], [29]. We performed SAR numerical analysis at 2.4 GHz using the same simulation scenario as in Fig. 2 via assumption of 1 W as the net input power. Fig. 11 shows the results, with 1-g averaged (IEEE C95.1-1999) and 10-g averaged (IEEE C95.1-2005) SAR values of 568.2 and 84.6 W/kg, accordingly. For patient safety, the net input power to reach SAR limits of 1.6 (IEEE C95.1-1999) and 2 (IEEE C95.1-2005) W/kg must be reduced from the preset 1 W to 2.8 mW (for 1 g) and 23.6 mW (for 10 g). The maximum average SAR values and maximum allowable net input power for both IEEE guidelines are summarized in Table 4. According to the authors in [9] and [14], there is a trade-off between the implantable antenna size and its SAR values. As shown in Table 5, note that our proposed antenna had a smaller size but higher SAR values than those in [25]–[27]. However, our maximum allowable net input power of 2.8 and 23.6 mW for the 1-g and 10-g standards was way higher compared to 3.2 μW (−25 dBm), which is the output power of most transmitters in implantable applications [24]. This means that, even though the transmitter produces an output power of 3.2 μW or higher as an input power for the implanted antenna, the SAR values would only reach 1.8 mW/kg (for 1 g) and 0.3 mW/kg (for 10 g), which are much smaller than the respective IEEE limits of 1.6 and 2 W/kg. Therefore, our SAR values should not be a concern in this communication.

IV. CONCLUSION

In this paper, a miniaturized implantable antenna and its characteristics while immersed inside a seven-layer brain phantom were presented. The proposed antenna exhibited a broadside radiation pattern and wide operating bandwidth which are crucial in brain signal transmission application in a wireless brain monitoring system. Unlike in free space, designing an implantable antenna in a human brain to have a broadside radiation characteristic is a very challenging point of interest because biological brain tissues have frequency-dependent electrical properties that can change the antenna performance. Therefore, a realistic brain model must be used to preserve the optimized broadside radiation characteristic of the antenna and achieve more realistic results. Moreover, patient safety as a priority restricts the many aspects of an implantable antenna design, including miniaturization, biocompatibility, and maximum input power.

In this work, we successfully designed an antenna that addressed all the main aspects. Furthermore, our work is the first to present a simplified and realistic brain model with seven tissue layers for antenna design and optimization. We also proposed and fabricated a seven-layer semi-solid ATE brain phantom for in-vitro measurement applications, mainly to check the performance of the fabricated antenna prototype. The measurement results confirmed that the antenna really radiated in a directional manner in the broadside direction. Both the measured and simulated results agreed well with each other. We also compared the overall performance of our proposed antenna with those in previous studies, in which we proved that our antenna exhibited a wider bandwidth than those of other single-band implantable antennas operating at 2.4 GHz, with satisfactory performance. With the proposed antenna, we are currently constructing a brain to off-body wireless communication link to perform the link budget analysis.

REFERENCES

[1] Y. Zhao, R. L. Rennaker, C. Hutchens, and T. S. Ibrahim, "Implanted miniaturized antenna for brain computer interface applications: Analysis and design," *PLoS ONE*, vol. 9, no. 7, Jul. 2014, Art. no. e103945.
[2] C. W. L. Lee, A. Kiourti, J. Chae, and J. L. Volakis, "A high-sensitivity fully passive neurosensing system for wireless brain signal monitoring," *IEEE Trans. Microw. Theory Techn.*, vol. 63, no. 6, pp. 2060–2068, Jun. 2015.
[3] W.-C. Chen, C. W. L. Lee, A. Kiourti, and J. L. Volakis, "A multi-channel passive brain implant for wireless neuropotential monitoring," *IEEE J. Electromagn., RF, Microw. Med. Biol.*, vol. 2, no. 4, pp. 262–269, Dec. 2018.
[4] L. Song and Y. Rahmat-Samii, "An end-to-end implanted brain–machine interface antenna system performance characterizations and development," *IEEE Trans. Antennas Propag.*, vol. 65, no. 7, pp. 3399–3408, Jul. 2017.
[5] C. W. Lee, "A wireless, fully-passive recorder for medical applications," Ph.D. dissertation, Dept. Elect. Comput. Eng., Ohio State Univ., Columbus, OH, USA, 2016.
[6] A. Kiourti, C. W. L. Lee, J. Chae, and J. L. Volakis, "A wireless fully passive neural recording device for unobtrusive neuropotential monitoring," *IEEE Trans. Biomed. Eng.*, vol. 63, no. 1, pp. 131–137, Jan. 2016.
[7] T. Seo, S. Oh, D. Jung, Y. Huh, J. Cho, and Y. Kwon, "Noninvasive brain stimulation using a modulated microwave signal," *J. Electromagn. Eng. Sci.*, vol. 18, no. 1, pp. 70–72, 2018.
[8] H. Bahrami, S. A. Mirbozorgi, R. Ameli, L. A. Rusch, and B. Gosselin, "Flexible, polarization-diverse UWB antennas for implantable neural recording systems," *IEEE Trans. Biomed. Circuits Syst.*, vol. 10, no. 1, pp. 38–48, Feb. 2016.
[9] A. Kiourti and K. S. Nikita, "A review of implantable patch antennas for biomedical telemetry: Challenges and solutions [wireless corner]," *IEEE Antennas Propag. Mag.*, vol. 54, no. 3, pp. 210–228, Jun. 2012.

[10] A. Kiourti, M. Christopoulou, and K. S. Nikita, "Performance of a novel miniature antenna implanted in the human head for wireless biotelemetry," in *Proc. IEEE Int. Symp. Antennas Propag. (APSURSI)*, Jul. 2011, pp. 392–395.
[11] A. Kiourti, J. R. Costa, C. A. Fernandes, A. G. Santiago, and K. S. Nikita, "Miniature implantable antennas for biomedical telemetry: From simulation to realization," *IEEE Trans. Biomed. Eng.*, vol. 59, no. 11, pp. 3140–3147, Nov. 2012.
[12] C. M. Lee, T. C. Yo, C. H. Luo, C. H. Tu, and Y. Z. Juang, "Compact broadband stacked implantable antenna for biotelemetry with medical devices," *Electron. Lett.*, vol. 43, no. 12, pp. 660–662, Jun. 2007.
[13] W.-C. Liu, F.-M. Yeh, and M. Ghavami, "Miniaturized implantable broadband antenna for biotelemetry communication," *Microw. Opt. Technol. Lett.*, vol. 50, no. 9, pp. 2407–2409, Sep. 2008.
[14] H. Bahrami, B. Gosselin, and L. A. Rusch, "Design of a miniaturized UWB antenna optimized for implantable neural recording systems," in *Proc. 10th IEEE Int. NEWCAS Conf.*, Jun. 2012, pp. 309–312.
[15] A. Drossos, V. Santomaa, and N. Kuster, "The dependence of electromagnetic energy absorption upon human head tissue composition in the frequency range of 300-3000 MHz," *IEEE Trans. Microw. Theory Techn.*, vol. 48, no. 11, pp. 1988–1995, Nov. 2000.
[16] S. Gabriel, R. Lau, and C. Gabriel, "The dielectric properties of biological tissues: II. Measurements in the frequency range 10 Hz to 20 GHz," *Phys. Med. Biol.*, vol. 41, no. 11, pp. 2251–2269, 1996. [Online]. Available: http://niremf.ifac.cnr.it/tissprop/
[17] H. Bahrami, B. Gosselin, and L. A. Rusch, "Realistic modeling of the biological channel for the design of implantable wireless UWB communication systems," in *Proc. Annu. Int. Conf. IEEE Eng. Med. Biol. Soc.*, Aug./Sep. 2012, pp. 6015–6018.
[18] S. Gabriel, R. W. Lau, and C. Gabriel, "The dielectric properties of biological tissues: III. Parametric models for the dielectric spectrum of tissues," *Phys. Med. Biol.*, vol. 41, no. 11, pp. 2271–2293, 1996.
[19] P. Soontornpipit, C. M. Furse, and Y. C. Chung, "Design of implantable microstrip antenna for communication with medical implants," *IEEE Trans. Microw. Theory Techn.*, vol. 52, no. 8, pp. 1944–1951, Aug. 2004.
[20] A. Kiourti and K. S. Nikita, "Miniature scalp-implantable antennas for telemetry in the MICS and ism bands: Design, safety considerations and link budget analysis," *IEEE Trans. Antennas Propag.*, vol. 60, no. 8, pp. 3568–3575, Aug. 2012.
[21] K. Ito, K. Furuya, Y. Okano, and L. Hamada, "Development and characteristics of a biological tissue-equivalent phantom for microwaves," *Electron. Commun. Jpn. I, Commun.*, vol. 84, no. 4, pp. 67–77, 2001.
[22] S. A. A. Shah and H. Yoo, "Scalp-implantable antenna systems for intracranial pressure monitoring," *IEEE Trans. Antennas Propag.*, vol. 66, no. 4, pp. 2170–2173, Apr. 2018.
[23] J.-H. Kim and B.-G. Kim, "Effect of feed substrate thickness on the bandwidth and radiation characteristics of an aperture-coupled microstrip antenna with a high permittivity feed substrate," *J. Electromagn. Eng. Sci.*, vol. 18, no. 2, pp. 101–107, Apr. 2018.
[24] Z. Duan, Y.-X. Guo, M. Je, and D.-L. Kwong, "Design and *in vitro* test of a differentially fed dual-band implantable antenna operating at MICS and ISM bands," *IEEE Trans. Antennas Propag.*, vol. 62, no. 5, pp. 2430–2439, May 2014.
[25] L.-J. Xu, Y. Bo, W.-J. Lu, L. Zhu, and C.-F. Guo, "Circularly polarized annular ring antenna with wide axial-ratio bandwidth for biomedical applications," *IEEE Access*, vol. 7, pp. 59999–60009, 2019.
[26] C. Liu, Y.-X. Guo, and S. Xiao, "Capacitively loaded circularly polarized implantable patch antenna for ISM band biomedical applications," *IEEE Trans. Antennas Propag.*, vol. 62, no. 5, pp. 2407–2417, May 2014.
[27] Z.-J. Yang, S.-Q. Xiao, L. Zhu, B.-Z. Wang, and H.-L. Tu, "A circularly polarized implantable antenna for 2.4-GHz ISM band biomedical applications," *IEEE Antennas Wireless Propag. Lett.*, vol. 16, pp. 2554–2557, 2017.
[28] *IEEE Standard for Safety Levels with Respect to Human Exposure to Radio Frequency Electromagnetic Fields, 3 kHz to 300 GHz*, IEEE Standard C95.1-1999, Apr. 1999.
[29] *IEEE Standard for Safety Levels with Respect to Human Exposure to Radio Frequency Electromagnetic Fields, 3 kHz to 300 GHz*, IEEE Standard C95.1-2005, Apr. 2005.

SAMNANG HOUT was born in Cambodia, in 1993. He received the B.S. degree in electronics engineering from Kangnam University, Yongin, South Korea, in 2018. He is currently pursuing the M.S. degree in integrated IT engineering with the Seoul National University of Science and Technology, Seoul, South Korea, where he is also a Research Assistant with the Electromagnetic Measurement and Application (EMMA) Laboratory. His current research interests include implantable antenna design, antenna theory, and brain phantom for in-vitro testing.

JAE-YOUNG CHUNG received the B.S. degree from Yonsei University, Seoul, South Korea, in 2002, and the M.S. and Ph.D. degrees from The Ohio State University, Columbus, OH, USA, in 2007 and 2010, respectively, all in electrical engineering. From 2002 to 2004, he was an RF Engineer with Motorola Korea. From 2010 to 2012, he was an Antenna Engineer with Samsung Electronics. He is currently an Associate Professor with the Department of Electrical and Information Engineering, Seoul National University of Science and Technology. His research interests include electromagnetic measurement and antenna design.